Nuclear Instruments and Methods 216 (1983) 35–44
North-Holland Publishing Company

THE ARGUS ELECTRON/PHOTON CALORIMETER
II. Properties of the light collection system of the lead/scintillator shower counters

A. DRESCHER, H.J. GRAF, B. GRÄWE, W. HOFMANN, A. MARKEES, U. MATTHIESEN, J. SPENGLER and D. WEGENER

Institut für Physik der Universität Dortmund, 4600 Dortmund 50, Fed. Rep. Germany

Received 31 March 1983

A detailed investigation is described of the photon production and transport in lead scintillator shower counters with wavelength shifter readout built for the ARGUS detector. Experimental data and Monte Carlo calculations are in good agreement. The most prominent effects due to the light collection system are small nonlinearities in the relation between deposited energy and pulse height and an energy dependent decrease of the energy resolution of the counters.

1. Introduction

The ARGUS detector, set up at the electron–positron storage ring DORIS at DESY, uses a modularized lead/scintillator shower counter to detect electrons and photons. The expected performance of this electron/photon calorimeter, as derived from test measurements of the counter modules, has been described in earlier publications [1–3]; typical energy resolutions of $7\%/\sqrt{E}$ and detection thresholds as low as 10 MeV were achieved.

Both the very fine sampling of showers, which is required in order to obtain such a performance, and the high degree of modularity of the calorimeter rely on the use of fluorescent radiation converters for the collection of scintillation light [4,5].

The method is illustrated in fig. 1. One side of a shower absorber, consisting of a stack of alternating layers of lead and scintillator, is covered with a lucite light guide doped with the fluorescent BBQ. The blue scintillation light leaves the scintillator plate at one edge, crosses a small air gap and enters the BBQ doped lucite light guide. It is then absorbed by the BBQ and reemitted isotropically as green light. A certain fraction of this reemitted light is trapped in the light guide and is transported to a phototube.

The aim of this investigation was twofold: first, it is known experimentally [3], that about 1.5 photoelectrons are produced at the cathode of the photomultiplier per MeV energy deposited in the calorimeter. The comparison of this number with the "theoretical" prediction allows to judge whether the calorimeter works as foreseen, or whether there are additional light losses due to imperfections in the material, of the surfaces, or due to tolerances in the assembly. Second, the efficiency of light collection varies over the sensitive volume of a calorimeter module. In order to correct for this effect, and hence to optimize the algorithms for reconstruction of particle energies and impact points, a detailed map of the collection efficiencies is required.

In this paper, we will present a quantitative description of the process of light production and -collection. Based on measurements of the relevant material parameters, a Monte Carlo simulation of the system of scintillator plates, wave-length shifter, and light guide was developed. Results of this model are compared to the

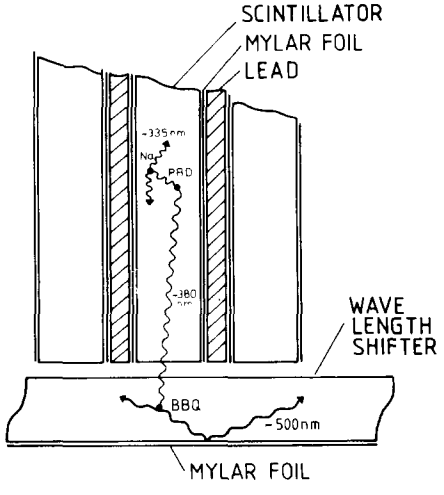

Fig. 1. Collection of scintillation light with a wavelength shifter bar:
Naphthalene (Na) : primary scintillator emitting UV light;
PBD : wavelength shifter UV-blue;
BBQ : wavelength shifter blue-green.

measured efficiencies of light collection, and their impact on linearity and energy resolution is discussed.

The paper is organized as follows: in section 2 we review the design of the calorimeter modules. Section 3 summarizes the measurements of material parameters, the numerical simulation of light transport, and the derived result for the mean number of photoelectrons. In section 4, the "efficiency map", and the implications of nonuniformities on the response of the shower counters are discussed. In section 5, time-of-flight measurements using the shower counters are described. A summary is given in section 6.

2. The lead/scintillator counter modules

Fig. 2 shows a schematic view of one of the shower counter modules used in the ARGUS "barrel" shower detector. Each module consists of two stacks of alternating plastic scintillator plates [6] and lead plates of 5 mm and 1 mm thickness respectively. The lead- and scintillator plates are separated by aluminized mylar foils with 98% reflectivity. The two stacks are read out separately via two wavelength shifter bars of 3 mm thickness [7] in the middle of each module coupled to 1" photo tubes [8] via adiabatic light guides [9]. The wavelength shifters are carefully shielded from each other by an aluminized mylar foil in order to eliminate crosstalk. A 0.3 mm nylon thread maintains the air gap between absorber stack and wavelength shifter. The whole module and the light guides are wrapped in aluminum foil (85%–90% reflectivity). The front end of the wavelength shifters is covered by an additional mylar foil. The mechanical stability of the module is provided by four layers of a special black thermal shrink tubing [10]. This procedure guarantees that the aluminium foil lies everywhere close to the edges of the scintillator and wavelength shifter plates.

All edges of the wavelength shifters and of the light guides were carefully machined and polished, but the scintillator plates were left unpolished. Earlier tests have shown [2], that polishing the edges gives no sizeable improvement in light output or homogeneity. This can be understood, since an unpolished edge backed up by aluminum foil more or less acts like diffuse reflector. Keil [4c] has shown that for the readout of scintillator plates (refractive index ~ 1.5) via an air gap both diffuse and specular reflectors of reflectivities around 0.8–0.9 give the same light output.

The length of the wavelength shifter bars exceeds the length of the absorber stack by about 2 cm. This feature offers two advantages: first, a quartz fiber cable can be installed at the rear end of the counter in order to supply a calibration pulse from the laser monitoring system (fg. 2) [11]; since this light is coupled into the wavelength shifter, the connection between shifter bar and light guide is tested as well. Second, the emission and absorption spectra of BBQ slightly overlap. Therefore photons within the overlap region are reabsorbed within a few centimeters, and give rise to a strong variation of light output with the distance from the light guide [4c]. In our case, the last centimeters of the wavelength shifter, which are not irradiated by scintillator light, act as filter smoothing the attenuation curve [4c].

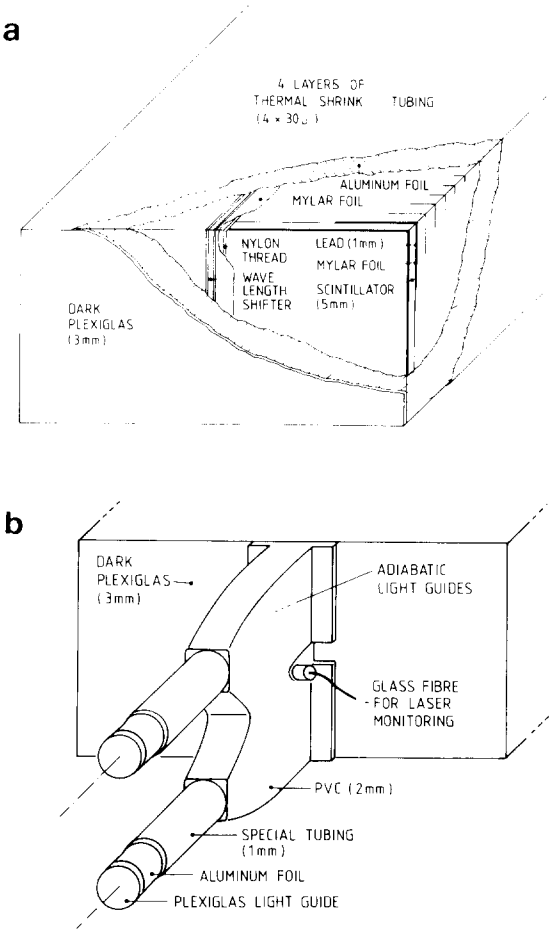

Fig. 2. Construction of a ("parallel") shower counter module: One module contains two stacks of lead- and scintillator plates, which are read out separately via two wavelength shifters. All edges are taped for extra protection. (a) Front end view, (b) rear end with light guides and monitor input.

In the ARGUS barrel shower counter, two types of calorimeter modules are used: in azimuth (φ) modules like the one shown in fig. 2 (the so-called "parallel' calorimeter modules) alternate with wedge-shaped modules (fig. 3). The use of two different types of modules (instead of one standard wedge module) is unavoidable, since the support structure has to be filled from the inside of the detector [12].

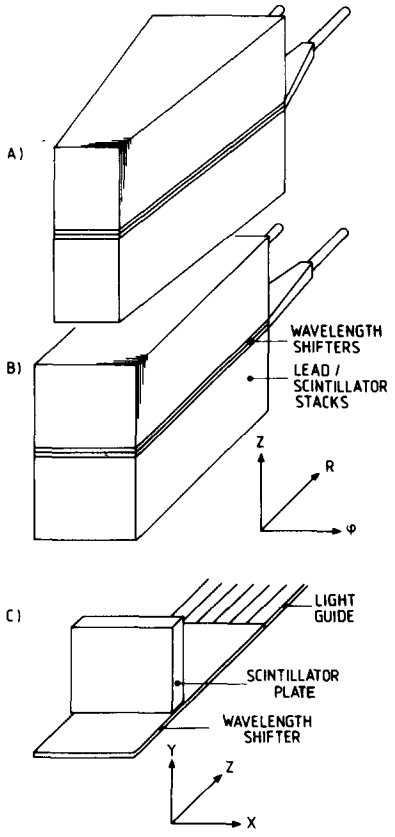

Fig. 3. Calorimeter modules used in the ARGUS "barrel" shower counter: "wedge" (a) and "parallel" (b). The coordinate system refers to the standard ARGUS coordinates: z is along the beam axis, r and φ are the radial and azimuthal coordinates, respectively. (c) Coordinate system used to describe the efficiency of photon collection, section 4.

Table 1
Dimensions of calorimeter modules.

Type	"Parallel"	"Wedge"
No. of lead plates	64	64
No. of scintillator plates	64	64
Thickness of lead plates (mm)	1	1
Thickness of scintillator plates (mm)	5	5
Length of entire stack (mm)	~ 390	~ 390
Length of entire stack (X_0)	12.4	12.4
z-extension of plates (mm)	103.4	103.4
φ-extension, first plate (mm)	108.7	69.9
φ-extension, last plate (mm)	108.7	147.1

Further information on the calorimeter modules is given in refs. 3 and 13.

3. Efficiency of light collection

In the following paragraph the expected number of photoelectrons produced at the photocathode of a photomultiplier attached to the light guide of a parallel module will be calculated.

For a given amount E_0 of energy deposited somewhere in a scintillator plate of a calorimeter module, the mean number of photoelectrons is

$$N_{\text{photoel}} = \epsilon E_0,$$

where

$$\epsilon = \int d\lambda_1 \int d\lambda_2 E(\lambda_1) \cdot T_1(\lambda_1) \cdot A_1(\lambda_1) \times W(\lambda_1, \lambda_2) \cdot T_2(\lambda_2) \cdot S(\lambda_2), \quad (1)$$

with

$E(\lambda_1)$: scintillator emission spectrum;
$T_1(\lambda_1)$: probability for light transmission from the production place in the scintillator via the air gap into the wavelength shifter;
$A_1(\lambda_1)$: probability that scintillator light is absorbed in the wavelength shifter;
$W(\lambda_1, \lambda_2)$: probability of emission of λ_2 by the BBQ after absorption of a photon λ_1;
$T_2(\lambda_2)$: probability for light transmission to the photomultiplier;
$S(\lambda_2)$: quantum efficiency of the photomultiplier.

$E(\lambda_1)$: The shape of the scintillator emission spectrum was measured using a Jarrel–Ash monochromator. In order to obtain the required intensities, the scintillator was excited by UV-light from a mercury–cadmium lamp. The apparatus was calibrated using the known [14] spectra of sodium salicylate and fluoranthene. The resulting spectrum is shown in fig. 4a; typical errors are ± 5 nm in λ and $\pm 2.5\%$ in the intensity. As compared to the emission spectra of pure PBD [14], the maximum of emission is shifted by 30 nm. This shift is likely to be caused by chemical effects due to the comparatively high concentration and due to the other additives. To determine the normalisation of E, i.e. the absolute photon yield per MeV deposited energy, a small piece of scintillator was coupled directly to a photomultiplier, and was excited by minimum ionizing particles. The number of photoelectrons seen was determined from comparison with a light emitting diode reference spectrum, assuming that the width of the Gaussian LED peak is proportional to $1/\sqrt{N_{ph.el.}}$, and taking into account the additional fluctuations in the first photomultiplier stages. Using the calculated geometrical efficiency of light collection, the average quantum efficiency of the photomultiplier as derived from the

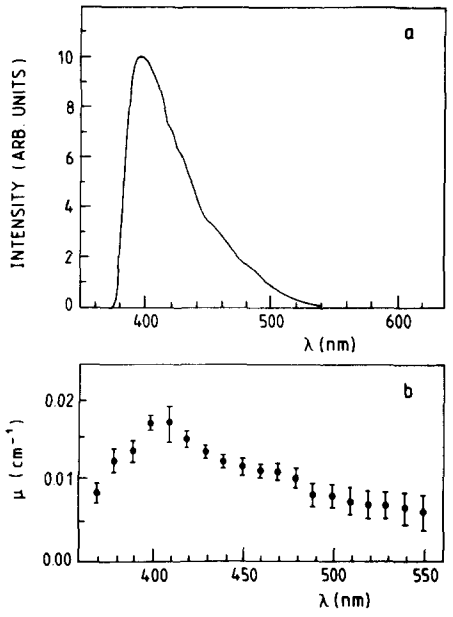

Fig. 4. (a) Spectrum of scintillator emission. (b) Absorption coefficients of scintillator material vs. wavelength.

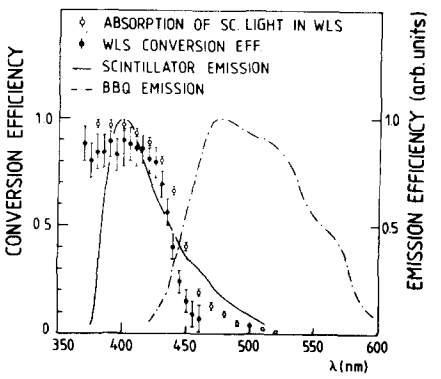

Fig. 5. Absorption of light in the wavelength shifter, and probability for reemission vs. wavelength of the incident light. For comparison, the emission spectra of scintillator and BBQ are included.

measured spectrum, and known cathode sensitivity [8], the mean number N_{sc}

$$N_{sc} = (2050 \pm 300) \text{ photons/MeV} \quad (2)$$

of photons per MeV energy deposited in the scintillator was obtained.

$T_1(\lambda_1)$: The coefficient T_1 depends on the geometrical probability, that a photon leaves the scintillator plate at the side of the wavelength shifter, and on the absorption length in the scintillator. Using a well collimated light beam, and scintillator blocks of different length, the absorption coefficients were measured (fig. 4b). The Monte Carlo method was used to determine T_1 by tracking a large number of photons, with a spectrum shown in fig. 3, which were assumed to be emitted isotropically, yielding

$$\langle T_1 \rangle = (0.18 \pm 0.03) \cdot (0.96 \pm 0.01) = 0.17 \pm 0.03, \quad (3)$$

averaged over a scintillator plate. The first term in eq. (3) accounts for the transport up the surface of the wavelength shifter, whereas the second term describes reflection losses at the surface. The large error in eq. (3) results from the uncertainty in the treatment of light reflection at the unpolished edges of the scintillator plates.

$A_1(\lambda_1)$: The absorption of scintillator light in the wavelength shifter was measured (fig. 5) by comparing light transmission through the wavelength shifter and through a similar plate of plexiglass, thereby eliminating the effect of reflections at the surfaces. From the data shown in figs. 4a and 5, the overlap between scintillator emission and BBQ absorption can be calculated to be (0.75 ± 0.04). The distortion of the scintillator spectrum due to the wavelength dependence of its absorption coefficient has been accounted for.

$W(\lambda_1, \lambda_2)$: For the determination of the conversion efficiency, a monochromatic light source was used to excite a small wavelength shifter plate directly coupled to a photomultiplier. The beam intensity was monitored via a beam splitter by a second photomultiplier, whose gain relative to the first one was known. With the measured BBQ emission spectrum (fig. 5), the known photocathode efficiencies, the absorption probability A_1 and the geometrical efficiency for light collection in the WLS-probe, the ratio of photon numbers in the beam and after the reemission can be determined. It is plotted in fig. 5, as a function of the wavelength of the exciting light. In addition to the errors shown in fig. 5,the reabsorption of photons in the overlap region between BBQ emission and -absorption introduces systematic effects. Due to the small size of the probe, however, this effect is expected to be almost negligible.

In the determination of W, the following assumption was made

$$W(\lambda_1, \lambda_2) = U(\lambda_1) \cdot V(\lambda_2), \quad (4)$$

i.e. the shape of the emitted spectrum is independent of the incident photon's wavelength. Explicit measurements have shown, that this is a reasonable approximation for $\lambda_1 < 425 \cdots 450$ nm, and it will be kept in all following calculations. Obviously, this introduces an incorrect treatment of photons in the tail of the scintillator emission spectrum; but since these photons anyhow are not likely to be absorbed, the error due to this approximation is negligible. Weighted with the spectrum of scintillator emission and BBQ absorption, a mean conversion efficiency of (0.76 ± 0.09) is obtained.

$T_2(\lambda_1)$: Similar to the determination of T_1, T_2 was

obtained by a Monte Carlo simulation of photon tracks in the wavelength shifter and in the adiabatic light guide. In order to account properly for the possible absorption of light in the wavelength shifter, the wavelength dependence of BBQ-emission and absorption was included. We used the emission spectrum shown in fig. 5. The absorption coefficients in the WLS were taken from [5c], and corrected for a BBQ-concentration of 120 mg/l. For a wavelength larger than ~ 470 nm, a constant absorption length of ~ 180 cm was used, as extrapolated from other measurements [4f].

The aluminum wrapping of the WLS was treated as a specular reflector with reflectivities of 0.85 at the sides, and a reflectivity R between 0 and 1 at the front end. The latter uncertainty is due to the fact that the construction of the shower counters sometimes allows for a small air gap between the front end of the WLS and the plexiglass front plate. In such a case, most of photons reflected back at the front-end mylar foil will miss the WLS. This uncertainty is included in the errors given below.

Furthermore it was assumed, that photons leaving the WLS towards the lead/scintillator stack are lost. All results however are fairly insensitive on these assumptions, except for the front-end reflectivity R.

The six fingers of the adiabatic light guide were simulated as straight pieces of plexiglas. Since the bending radius of the strips is large compared to the strip thickness; additional losses should not exceed 10% [15]. The transmission of light through the light guide was measured to be homogeneous within 3%. Further details will be given in section 4. For the average T_2 one obtains

$$T_2(0.25 \pm 0.03) \cdot (0.95 \pm 0.05) = (0.24 \pm 0.03). \quad (5)$$

The first term refers to the collection efficiency as derived from the Monte Carlo model, the second term accounts for losses in the non-ideal light guide.

$S(\lambda_2)$: From the integral over the photon spectrum, weighted with the quantum efficiency [8] of the Cs–Sb photocathode, a mean conversion efficiency for photons of

$$S = (0.12 \pm 0.01) \quad (6)$$

is obtained. From the evaluation of eq. (1), we therefore predict a yield of

$$\epsilon = (5.7 \pm 1.7 \text{ photoelectrons})/(\text{MeV deposited energy}).$$

This result can be compared to the number of photoelectrons produced by an electromagnetic shower. In ref. 3 (1.5 ± 0.3) photoelectrons per MeV energy of a primary electron hitting a shower counter were observed. Since for electromagnetic showers roughly 30% of the primary electron energy is deposited in the scintillator [3], this corresponds to (5 ± 1) photoelectrons per MeV in the scintillator. This number is in good agreement with the result of the present study and proves that the light production and collection properties of the shower counters are quantitatively understood.

4. Response of the calorimeter to electromagnetic showers

The efficiency of light collection, as derived in section 3, refers to the production of scintillation light at a fixed place in the absorber stack; the final result has been averaged over the entire active volume of a module. Detecting electron- or photon showers, we face a somewhat different situation: the energy deposition in a shower creates a number of distributed light sources. Let $\delta(x, y, z)$ be the energy deposition per unit volume of scintillator. Then we have

$$N_{\text{photoel}} = \int \mathrm{d}x\mathrm{d}y\mathrm{d}z\epsilon(x, y, z) \cdot \delta(x, y, z), \quad (7)$$

with the efficiency ϵ as defined in section 3. For definiteness, choose x, y, z as shown in fig. 3c, and consider a shower whose axis in parallel to z. Any dependence of ϵ on x and y means that the response of the calorimeter is nonuniform and depends on the impact point of a particle. Any z-dependence of ϵ, on the other hand, introduces nonlinearities in the energy calibration of the shower counter, since the shape of the longitudinal profile of a shower,

$$\delta(z) = \int \mathrm{d}x\mathrm{d}y\delta(x, y, z) \quad (8)$$

changes with the energy E of an incident particle, and correspondingly the weighted mean efficiency $\langle\epsilon\rangle$

$$\langle\epsilon\rangle = \frac{\int \mathrm{d}x\mathrm{d}y\mathrm{d}z\epsilon(x, y, z) \cdot \delta(x, y, z)}{\int \mathrm{d}x\mathrm{d}y\mathrm{d}z\delta(x, y, z)} \quad (9)$$

becomes a function of energy. The variation of $\langle\epsilon\rangle$ is relatively small, and can be neglected in considerations such as presented in section 3; nevertheless it is an important effect in high-precision energy measurements with a shower detector.

Furthermore, a nonuniformity of ϵ produces a deterioration of the effective energy resolution, since any fluctuation in the development of a shower is immediately translated into a fluctuation of $\langle\epsilon\rangle$.

Before going into a detailed discussion, let us recollect the limits beyond which inhomogeneities in the light collection start to harm the energy resolution of the calorimeter. Obviously, the effect is most critical at high energies, since there the resolution limit due to sampling fluctuations is small; all energy-independent contributions gain in importance. At the top energy of DORIS II of 5 GeV to 6 GeV, the resolution of a counter module is about 3.5–4% rms [3]. Consequently, light collection becomes a critical factor, once the rms

fluctuation of ϵ, measured in the region of the counters where the energy deposition is high, i.e. in the first half of a stack, exceeds this value. In fact, the observation of irregularities in the energy calibration and in the energy resolution led us to a detailed study of the optical system.

$\epsilon(x, y, z)$ has been determined experimentally by irradiating the scintillator at a well defined position by a high-intensity beta-source, and measuring the dc anode current of the photomultiplier.

In order to reduce the number of measurements, and to simplify the presentation of data, we assumed the transport efficiency of scintillator light can be factorised as

$$\epsilon(x, y, z) = \epsilon_1(x, y) \cdot \epsilon_2(z). \tag{10}$$

The term ϵ_1 describes the transport of photons from the place of production in the scintillator to the wavelength shifter, and the term ϵ_2 represents the collection of photons in the wavelength shifter. This type of factorising is exact provided that the efficiency of transport in the wavelength shifter does not depend on the transverse coordinate x of the point at which a blue photon hits the wavelength shifter. Geometrical considerations suggest such a behaviour. Experimentally, eq. (10) was approximately fulfilled, deviations occur at the 1–2% level and are negligible.

ϵ_1: fig. 6 shows the dependence of ϵ_1 on x (coordinate parallel to the wavelength shifter surface) and y (distance from the wavelength shifter), for a scintillator plate of a parallel module. As expected, the x-dependence is weak ($\sim 3\%$ rms) and just below the critical limit.

The y-dependence is much stronger ($\sim 11\%$ rms), and has to be corrected in practical applications using the reconstructed impact position of a particle [3]. ϵ has also been calculated by Monte Carlo tracking of photons, the results are included in fig. 6 as full lines. The absolute efficiency values given by the right-hand scale refer to the Monte Carlo and describe the transport-probability up the wavelength shifter surface. The slight discrepancy between Monte Carlo and data at $y \sim 0$ probably results from the transmission and conversion of primary UV-light to the wavelength shifter, which was not considered in the Monte Carlo calculation.

Since ϵ_1 depends somewhat of the size of a scintillator plate, it differs for the various plates in a wedge module (see table 1). According to the Monte Carlo simulation, the maximum value of ϵ_1 increases from 17.3% for the first (small) plate to 18.0% for the last (large) plate. This variation, however, corresponds to a 1%rms change in ϵ_1 and is negligible.

ϵ_2: The result of a Monte Carlo calculation of $\epsilon_2(z)$ is presented in fig. 7, for both parallel and wedge wave length shifters, and for reflectivity 1 of the external reflector at the end of the wavelength shifter opposite to the light-guide. The two types are seen to behave drastically different. Whereas the wavelength shifter of a parallel module exhibits a very smooth and almost constant efficiency in the critical region around the shower maximum, the efficiency of the wedge wavelength shifter has a pronounced z-dependence.

The model can be used to trace the origin of the difference between parallel and wedge wavelength shifters. The major differences arise in the losses at the y–z sides, and in the losses in the light guides. The explanation is simple: in the wedge wavelength shifter, each reflection of photons at the y–z sides leads to an alignment of photons along the z-axis, thereby reducing the mean path length and the number of reflections, and hence the losses. On the other hand, photons which are trapped in a wedge wavelength shifter by total reflec-

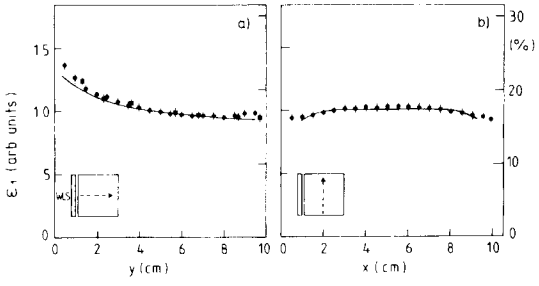

Fig. 6. Efficiency of light transport in a scintillator plate: shown is the efficiency of light transport from a production place in the scintillator to the surface of the wavelength shifter bar. (a) As a function of the distance y from the wavelength shifter. Circles refer to data obtained using a high intensity source and measuring the mean dc anode current, square points denote the peak of the pulse height distribution by minimum ionizing particles. (b) As a function of the coordinate x, at a distance of 5 cm from the wavelength shifter.

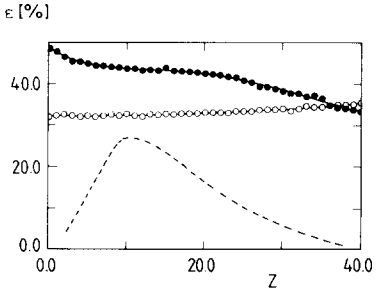

Fig. 7. Efficiency of light transport in the wavelength shifter: Result of a Monte Carlo calculation of the efficiency for light transport from the place of reemission in the wavelength-shifter bar to the photocathode, as a function of z: ○ parallel counters, ● wedge counters. For comparison, the longitudinal profile of the energy deposition by a 1 GeV electron shower is included.

tion, are not necessarily also trapped in the light guide; therefore the losses in the light guide are larger in the wedge counters for photons produced close to the beginning of the light guide.

Do these imperfections of the light collection system provide a quantitative explanation for the measured deviations from homogeneity and linearity of the shower counters? Consider first the spatial homogeneity. Fig. 8 shows the mean pulse height as a function of the impact position for 32.5 MeV electrons [3]. The direction of the electrons coincides with the z-axis. The beam was scanned in x-direction from the wavelength shifter of one module across the gap between two counters to the wavelength shifter of the next module.

The response of the calorimeter is seen to vary by 30%. These experimental results are compared to model predictions. They were obtained by integrating the lateral energy deposition in electromagnetic showers weighted with the efficiency ϵ_1. In agreement with measurements, ϵ_1 was assumed to factorize as

$$\epsilon_1(x,y) = \epsilon_{1x}(x) \cdot \epsilon_{1y}(y), \tag{11}$$

with $\epsilon_{1x,y}$ as displayed in fig. 6. The result is included in fig. 8 (full line). Slight discrepancies close to the wavelength shifters are probably due to shower particles generating Cherenkov-light in the wavelength shifters, an effect not included in the simulation.

As already mentioned, the z-dependence of ϵ_2 will introduce nonlinearities of the energy dependence. In order to simulate this effect, $\langle\epsilon\rangle$ has been calculated for different energies. For $\delta(z)$ a parametrisation based on results from the EGS Monte Carlo code [16] was used

$$\delta(t) = At^{0.561nE+1.92}e^{-0.575t}, \tag{12}$$

$t = z/X_0$ (E in GeV, X_0 = radiation length).

Fig. 9a shows $\langle\epsilon\rangle$ vs. energy for parallel and wedge counter modules. For the wedge modules $\langle\epsilon\rangle$ decreases with energy, whereas the parallel modules show the opposite behaviour.

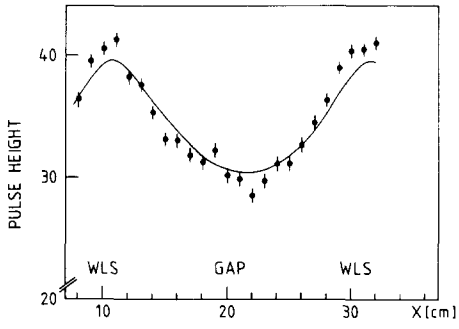

Fig. 8. Mean pulse height visible in a calorimeter array as a function of the impact position of the 32.5 MeV electron beam [3] compared to the simulation based on the efficiencies shown in fig. 6.

Besides the efficiency changes, another effect introduces nonlinearities: due to the finite length of the counters, the losses due to longitudinal leakage increase with energy; fig. 9a includes a curve demonstrating this effect. The leakage losses tend to increase the nonlinearity of wedge counters, whereas for parallel modules effects of light collection and leakage partly cancel; the resulting net nonlinearities are shown in figs. 9b and c, and are compared with data from recent calibration runs at DESY. In the energy range required for ARGUS, 50 MeV $\leqq E \leqq$ 5 GeV, typical nonlinearities in the uncorrected calorimeter data will be about -4% to 1% for the parallel, and slightly larger (10% to -1%) for the wedge modules (always normalized to 3 GeV electrons).

The influence of the z-dependence of photon detection efficiencies on the energy resolution of the counters can be understood on the bases of a simple model: in earlier papers [2,3] it was argued that the energy dependence of the normalized energy resolution $\sigma\sqrt{E}$ results from an interplay of two components. Sampling fluctuation and photoelectron statistics behave like $\sigma \propto 1/\sqrt{E}$, yielding $\sigma\sqrt{E}$ = const. $\approx 6.5\%$ at low energies [3]. In addition, fluctations in the containment of showers in the calorimeter have to be considered. In a very crude approximation, the dominant contribution due to leakage at the rear end of a module is given by

$$\Delta E = \Delta t (\mathrm{d}E/\mathrm{d}t)|_{t_0}, \tag{13}$$

where $(\mathrm{d}E/\mathrm{d}t)|_{t_0}$ is the mean energy deposition per radiation length at the end t_0 of the absorber, and $\Delta t \approx 1$ rad. length is the fluctuation of the shower center [2]. The physical idea behind formula (13) is that depending on the position of the first conversions in the shower, the whole cascade moves forward or backward within the absorber. If we neglect the weak energy dependence of the shower profile, eq. (13) results in an energy independent contribution to the relative resolution:

$$\Delta E/E = \Delta t f(t)|_{t_0} \approx 2.5\%, \tag{14}$$

with $(\mathrm{d}E/\mathrm{d}t) = Ef(t)$. Since the resolution limit due to sampling fluctuations becomes smaller and smaller as energy increases, eq. (14) finally dominates, and we obtain $\sigma\sqrt{E} \propto \sqrt{E}$.

Especially for wedge counters, however, also the mean efficiency for photon collection changes with the shower position, and generates a third contribution to the energy resolution

$$\frac{\mathrm{d}N_{\mathrm{photoel}}}{N_{\mathrm{photoel}}} = (1/\langle\epsilon\rangle) \cdot (\mathrm{d}\epsilon/\mathrm{d}t) \cdot \mathrm{d}t, \tag{15}$$

(N_{photoel} = number of photoelectrons).

Taking the average $\mathrm{d}\epsilon/\mathrm{d}t$ in the region of the shower

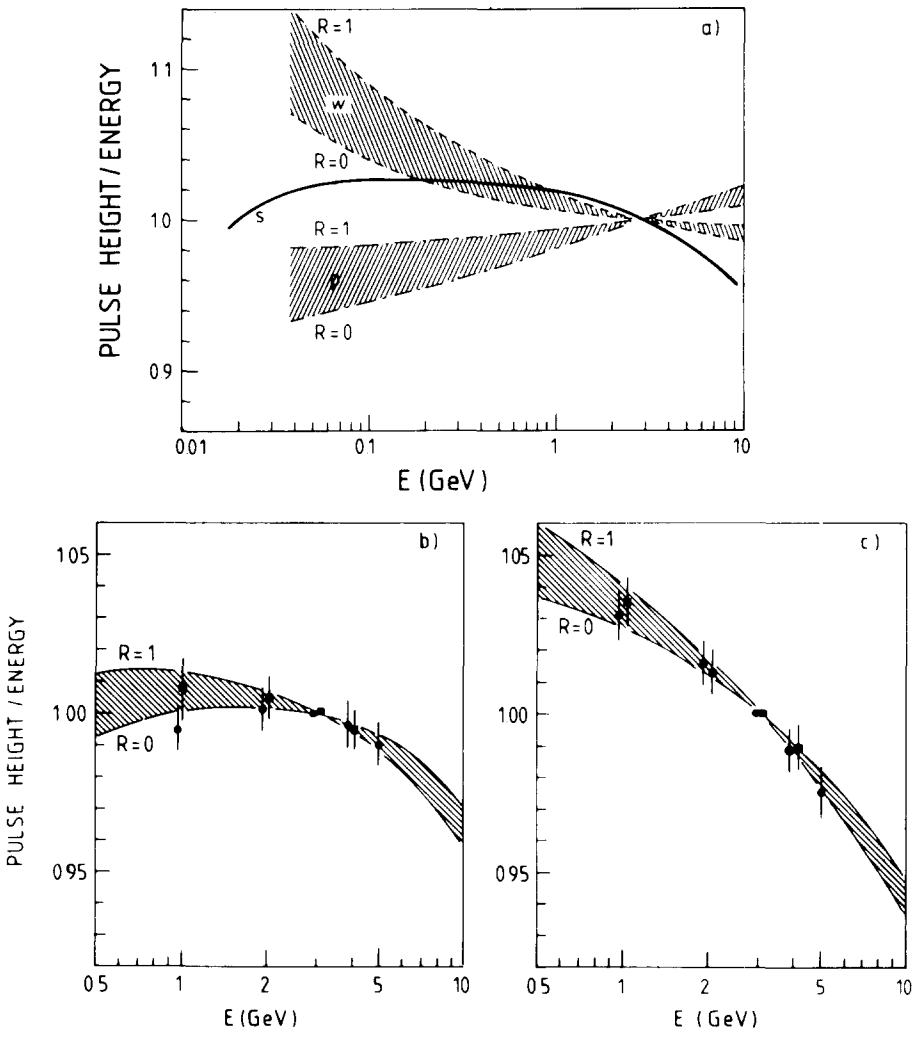

Fig. 9. Nonlinearities: Contributions to nonlinearities in the energy calibration of the shower counters; shown is always the amount of light seen by the photomultiplier per unit incident energy. All curves are normalized to 1 at $E_0 = 3$ GeV. $R = 0$ and $R = 1$ refer to wavelength shifters without and with front end specular reflectors, respectively. (a) Energy dependence of the efficiency for light collection "parallel" counters: area labeled "P", "wedge" counters: area labeled "W". Also included: energy dependence of the fraction of energy deposited in the calorimeter module (curve labeled "S"). (b) Resulting nonlinearities for parallel counters. (c) Resulting nonlinearities for wedge counters. Areas "P" and "W" are derived using analytical expressions for the average shape of electromagnetic showers, and exploiting the measured efficiency of light collection (fig. 7). Circles and squares refer to measured nonlinearities based on 640 final calorimeter modules, and on 36 prototype counters, respectively.

maximum ($t \approx 4$), and $\Delta t \approx 1$, we get

$$\frac{\mathrm{d}N_{\mathrm{photoel}}}{N_{\mathrm{photoel}}} \approx 1.2\% \qquad (16)$$

for wedge modules.

For parallel modules, the effect is negligible, and even tends to compensate the effects of leakage. If we consider the processes as statistically independent (which is probably not fully legitimate for the latter two), the effective resolution is given by the quadratic sum of the three terms. The x-dependence of ϵ_1 can be neglected in this context, since data refer to measurements for fixed impact, and since most of the energy is deposited close to the shower axis.

Fig. 10 shows the measured normalized energy resolutions for parallel and wedge modules. The values shown represent averages over 640 counters, and refer to the σ obtained from a Gaussian fit to the distribution of pulse heights. Only data within $\pm 1\sigma$ around the most probable value were considered for the determination of the widths.

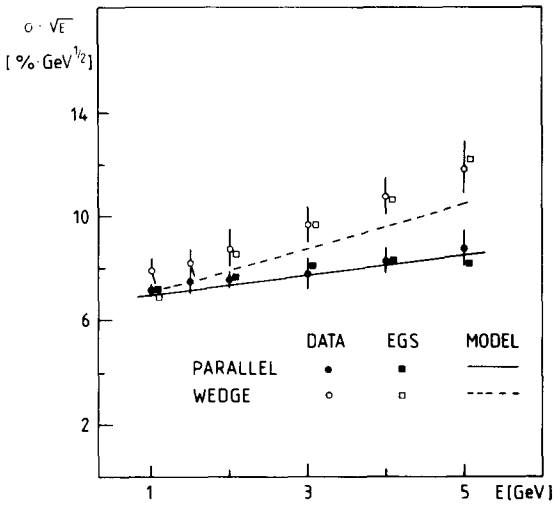

Fig. 10. Energy resolution: Normalized energy resolution $\sigma\sqrt{E}$ of parallel and conical modules, averaged over 640 counters each. The values were obtained from a Gaussian fit $\pm 1\sigma$ around the peak of the pulse-height distribution. The full lines refer to predictions based on a simple model discussed in the text; the rectangular points result from Monte Carlo simulations with the EGS code, including the efficiencies for photon transport shown in fig. 7.

The data show the expected trend: especially at high energies, in the region where leakage and fluctuations of the photon collection dominate the wedge modules are worse than the parallel ones. The trend of the data is well described by the simple model discussed above, and agrees with more elaborate calculations using the EGS code and the precise shape of the collection efficiencies.

5. Time resolution

For some purposes, like the detection of antibaryons annihilating in the shower counters, one might be interested to employ the shower counters also for time-of-flight measurements.

Various components contribute to the time resolution of such a system:

- lifetime of the excited states of the primary scintillator,
- decay time of the BBQ fluorescence,
- path length straggling of photons,
- differences in the transit time of photoelectrons in the photomultiplier.

The influence of the first three processes, up to the production of photoelectrons, has been investigated by a Monte Carlo simulation. The BBQ emission – two components with lifetimes of 17.9 and 620 ns respectively [4f] – turns out to be by far the dominant effect.

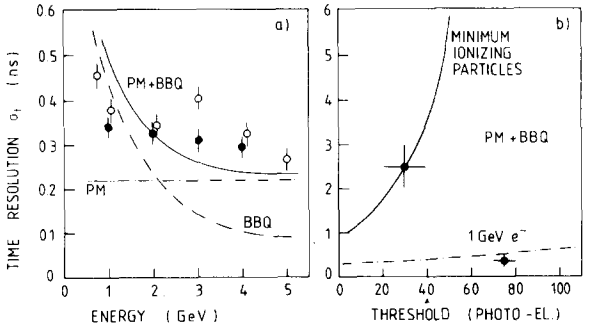

Fig. 11. Time resolution. (a) Time resolution of the calorimeter as a function of the electron energy, for a "parallel" (closed points) and a "wedge" (open points) module. Timing threshold at 5% of mean pulse height. Model predictions: dashed–dotted line: contribution from reemission and light collection; dashed–dotted–dotted line: limitation of time resolution due to photomultiplier; full line: quadratic sum of the two components. (b) Dependence of time resolution on the threshold setting. Points: "parallel" counter module; lines: model predictions.

Both experimental and model results on the time resolution of the calorimeter are shown in figs. 11a and b, as a function of the electron energy, and of the threshold setting of the discriminator generating the TDC signal, respectively.

Typical resolutions of 300–400 ps (Sigma of a Gaussian fit to the time-distribution) are obtained for electrons in the GeV region, with a weak energy dependence. The model calculations include two components: the time jitter produced in the light-transport system, i.e. mainly in the wavelength shifting process, and the jitter given by the photomultiplier, which was measured to be 220 ps almost independent of the light intensity, once the photoelectron number exceeds 1000. The model reproduces the main features of the measured resolutions, however the energy dependence seems slightly too steep.

6. Conclusions

The process of photon production and transport in the ARGUS lead/scintillator calorimeter has been investigated in detail both from the experimental and theoretical side. The agreement between results of the Monte Carlo simulation and the experimental data is satisfactory; in this sense the counters are fully "understood." The most prominent effects arising from properties of the light collection system are nonlinearities in the energy calibration of the calorimeter, and a worsening of the energy resolution. Both effects are more severe in the case of the "wedge" modules; for the "parallel" modules, distortions due to photon transport

and due to shower leakage even tend to cancel each other, resulting in a slight net improvement of the linearity.

We thank Prof. D. Fröhlich who made the spectrograph for the optical measurements available. His advice in optical problems was of great importance for us. We want to thank Prof. K.R. Schubert and R. Heller; we have greatly profited from their help during the tests, and from many interesting discussions. We acknowledge the skillful work of our technicians H. Höper, G. Metze and of our mechanical workshop in building the shower counters. One of us (W.H.) wants to thank the Deutsche Forschungsgemeinschaft for a Heisenberg Fellowship.

This work was supported by the Bundesministerium für Forschung und Technologie of the Federal Republic of Germany.

References

[1] W. Hofmann et al., Nucl. Instr. and Meth. 163 (1979) 77.
[2] W. Hofmann et al., Nucl. Instr. and Meth. 195 (1982) 475.
[3] A. Drescher et al., Nucl. Instr. and Meth. 205 (1983) 125.
[4] (a) W.A. Shurcliff, J. Opt. Soc. Am. 41 (1951) 209;
(b) R.C. Garwin, Rev. Sci. Instr. 31 (1960) 1010;
(c) G. Keil, Nucl. Instr. and Meth. 89 (1970) 111;
(d) W. Selove et al., Nucl. Instr. and Meth. 161 (1979) 233;
(e) W.B. Atwood et al., SLAC-TN-76-7 (1976);
(f) P. Klasen et al., Nucl. Instr. and Meth. 185 (1981) 67.
[5] (a) V. Eckardt et al., Nucl. Instr. and Meth. 155 (1978) 389;
(b) V. Bharadway et al., Nucl. Instr. and Meth. 155 (1978) 411;
(c) O. Botner et al., Nucl. Instr. and Meth. 179 (1981) 45;
(d) P. Rapp et al., Nucl. Instr. and Meth. 188 (1981) 445;
(e) M.A. Schneegans et al., Nucl. Instr. and Meth. 193 (1982) 445.
[6] ALTUSTIPE UV 15105, 84% PMMA, 15% Naphthalene, 1% Butyl-PBD, Altulor, Paris la defense, France.
[7] Plexiglas 218, 120 mg BBQ/l, Röhm GmbH, Darmstadt, FRG.
[8] PM XP 2008 UB, Valvo, Hamburg, FRG.
[9] Fa. Felder, Wuppertal, FRG.
[10] NALOPHAN, Kalle AG, Wiesbaden, FRG.
[11] R. Heller, Description of the optical monitoring system for the photomultipliers in ARGUS, IHEP Heidelberg, IHEP-HD/ARGUS/81-1.
[12] ARGUS, a new detector for DORIS, DESY Internal Report F15/PRO 148 (1978).
[13] A. Markees et al., to be published.
[14] I.B. Berlmann, Handbook of fluorescence spectra of aromatic molecules (Academic Press, New York, 1971).
[15] T. Massam, Nucl. Instr. and Meth. 141 (1977) 251.
[16] R.L. Ford and W.R. Nelson, SLAC-210, UC-32 (1978).